ARTICLES

Spectroscopy and Photophysics of Low-Lying Excited Singlet States of α,ω-Dithienylbutadiene and α,ω-Dithienylethylene Vapors

Takao Itoh*,† and Yasushi Numata‡

Graduate School of Integrated Arts and Science, Hiroshima University, 1-7-1 Kagamiyama, Higashi-Hiroshima City, 739-8521 Japan, and Department of Materials Chemistry and Engineering, College of Engineering, Nihon University, Koriyama, 963-8642 Japan

Received: February 9, 2009; Revised Manuscript Received: August 2, 2009

Fluorescence and excitation spectra and fluorescence lifetimes have been measured for α,ω-dithienylbutadiene (DTB) and α,ω-dithienylethylene (DTE) in a jet-cooled He expansion and in the static vapor phase. It is shown that the emission of DTB in the static vapor phase consists of the $S_1(2^1A_g)$ and $S_2(1^1B_u)$ fluorescence, while the emission in a jet consists of solely the S_1 fluorescence. The fluorescence quantum yields of DTB and DTE vapors decrease significantly with increasing excitation energy. The conformer-specific fluorescence was measured for DTB and DTE in a jet. The false S_1 (2^1A_g) origin of the most stable conformer of DTB was observed at 25470.5 cm^{-1} in a jet, which is located approximately 2800 cm^{-1} below the S_2 (1^1B_u) origin. The S_1 origins of the two conformers of DTE were observed at 28648 and 28966 cm^{-1} in a jet, and the S_1 state of the most stable conformer is assigned as 1^1B_u.

1. Introduction

Linear polyenes are prototypes of the π-electron conjugation systems for which a number of spectroscopic studies have been carried out since around the 1930s. It was known that linear polyenes exhibit an intense absorption band based on an allowed electronic transition, $1^1A_g \rightarrow 1^1B_u^*(\pi, \pi^*)$, the excitation energy of which decreases significantly with increasing polyene-chain length. In 1972, however, the existence of an optically forbidden ^1A_g excited state located below the 1^1B_u state was pointed out by Hudson and Kohler.[1−3] Since that time, a number of studies concerning the low-lying $2^1A_g^*(\pi, \pi^*)$ state of polyenes have been carried out. At present, the presence of the 2^1A_g state has been verified for a number of polyenes including unsubstituted, α,ω-dimethyl and α,ω-diphenylpolyenes.[1−15] α,ω-Dithienylpolyenes [(C_4H_3S)−$(CH{=}CH)_n$−(C_4H_3S)] also can be regarded as one of the substituted polyenes, and the fluorescence and excitation spectra have been reported in a low temperature *n*-alkane matrix and in room-temperature solution.[16−19] These spectra show clearly the presence of the 2^1A_g state for dithienylpolyenes, although the 2^1A_g and 1^1B_u states are nearly degenerate for α,ω-dithenylbutadiene (DTB) in a low temperature matrix.[16] In a previous paper, it was shown that the emission of dithenylbutadiene consists of the S_2 and S_1 fluorescence, while the emission of dithienylethylene (DTE) consists of solely the S_1 fluorescence in solution and in the static vapor phase.[19] In order to gain deeper insight into the low-lying electronic states of dithienylpolyenes, it is of importance to obtain vibrationally resolved optical spectra in the vapor phase where the molecules are not influenced by the environment. In contrast to diphenylpolyenes, dithienylpolyenes are considered to possess three rotational isomers, but the presence of the rotamers was not taken into account in the previous analyses.[19] Further, it is of interest to know the state ordering between the 2^1A_g and 1^1B_u states for dithienylethylene vapor and to compare the photophysics in the static vapor phase at low pressure and those in a jet. In the static vapor phase, the molecules are normally in thermodynamic equilibrium, while in a jet the molecules are cooled by expansion, providing the sharp spectra. The content of the previous paper is concerned with the photophysics of DTE and DTB in the static vapor phase at high total pressure and in solution.[19]

In the present work, fluorescence and fluorescence excitation spectra have been measured for *trans*-1,4-di(2-thienyl)-1,3-butadiene and *trans*-1,2-di(2-thienyl)ethylene in a jet cooled He expansion as well as in the static vapor phase. The conformer-specific fluorescence was measured for DTB and DTE in a jet. With DTB vapor, the $S_1(2^1A_g)$ state is observed clearly at energies below the allowed S_2 (1^1B_u) state in a jet. It is shown that the S_2 fluorescence appears as a weak emission band on the high-energy side of the S_1 fluorescence for DTB in the vapor phase, while only the S_1 fluorescence appears in a jet. By measuring and fitting the temperature dependence of the fluorescence spectrum of DTB in the static vapor phase, we are able to show that the emission originates from the S_2 state which is in thermodynamic equilibrium with the S_1 state. With DTE vapor, the measured fluorescence spectra are shown to originate from the S_1 state and the two stable conformers are identified in the excitation and fluorescence spectra in a jet. The S_1 origins of the two conformers were observed at 28648 and 28966 cm^{-1}.

* To whom correspondence should be addressed. E-mail: titoh@hiroshima-u.ac.jp.
† Hiroshima University.
‡ Nihon University.

10.1021/jp901180a CCC: $40.75
Published on Web 08/27/2009

2. Experimental and Computational

Materials and Apparatus. DTB and DTE were purified, and the purity was confirmed in the same ways as described in a forgoing paper.[19] Perfluorohexane obtained from Aldrich was used as a buffer gas without purification, after we confirmed that it contained no impurities that emitted under the conditions of our experiments.

The apparatus used for generating the supersonic free jet is almost the same as that described previously.[20] The samples seeded in helium gas with the pressure of 4 atm were heated up to 100−180 °C. The pulsed jet of the sample vapor was expanded into a vacuum chamber at 2.0×10^{-6} Torr through a nozzle (General Valve Series 9 with a 0.8 mm diameter). A frequency doubled dye laser (Spectra Physics, PDL-II) pumped by the third harmonic of the Nd:YAG laser (Powerlite 8000) was used as the exciting light source, which shows the typical bandwidth of 0.5 cm^{-1}. Wavelength calibration for the fluorescence excitation spectrum was carried out by simultaneous observation of atomic lines of Ar discharged inside a hollow-cathode lamp (Hamamatsu, L2483-26AR-FE). The laser beam was crossed with the jet at 12 mm downstream. The laser intensity was monitored by a pin photodiode after passing the jet and kept constant during the scanning. All of the wavelength values were corrected to those in a vacuum. During the measurement of the fluorescence excitation spectra, the scattered laser light was eliminated using a glass filter (Toshiba L-42) which has the window from 400 to 800 nm. The signals were averaged by a boxcar-integrated averager (Stanford Research SR-250). The dispersed fluorescence spectra were obtained by passing the emission through a 0.75 m monochromator (Nalumi-750). The signals were detected with a Hamamatsu R-928 photomultiplier equipped with a cooling system and accumulated by the same integrator system as that used for measuring the fluorescence excitation spectra. Fluorescence lifetimes in a jet were measured with a digital oscilloscope (Tektronix TDS744A) triggered by the exciting laser light.

Samples in the static vapor were prepared almost in the same way as described in a forgoing paper.[19] Absorption spectra were measured with a Shimadzu UV-2550 spectrophotometer and emission and excitation spectra were measured with a Spex Fluorolog-3 (model 21-SS) spectrophotometer for the static vapor samples. Two reflecting mirrors were placed beside the sample cell to intensify the emission signals.[21] Fluorescence spectra of the static vapor samples were corrected for the spectral sensitivity of the detection system by comparing the measured spectrum with the real spectrum using *N*,*N*-dimethylnitroaniline as a standard which shows emission ranging from 12000 to 22000 cm^{-1} in a hexane−benzene mixture.[22] Fluorescence spectra ranging from 18000 to 25000 cm^{-1} were corrected using quinine in sulfuric acid as a standard. Excitation spectra were corrected for the spectral intensity distribution of the exciting light using an aqueous solution of rhodamine B as a quantum counter.

Calculations. Quantum chemical calculations were carried out not only with the density-functional theory (DFT) method but also with semiempirical SCF-MO methods at the AM1, PM3, and INDO/3 levels. The DFT calculations were carried out using the Gaussian 03 program.[23] Optimized geometry, total energies, and harmonic vibrational wavenumbers of the ground-state molecules were obtained by DFT calculations at the B3LYP/6-311++G** level. The harmonic wavenumbers, ν_{harm}, in the ground state were scaled by the relation $\nu_{calc} = \nu_{harm} \times (1.0087 - 0.0000163 \times \nu_{harm})$ to reproduce the observed frequencies.[24]

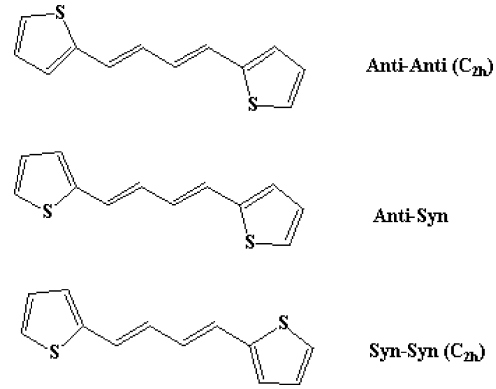

Figure 1. Molecular structure of DTB with the symmetries shown in parentheses. The same conformations apply for DTE.

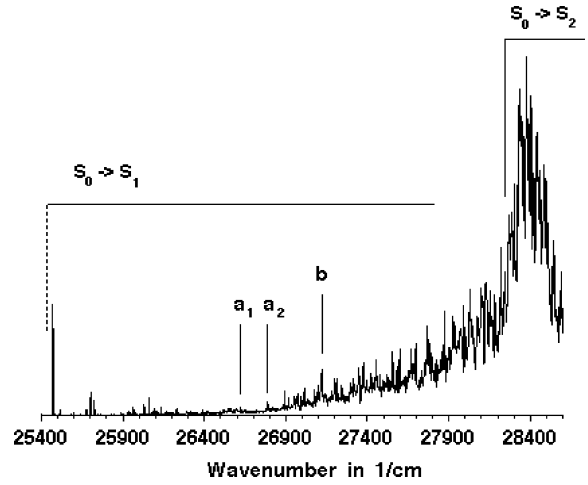

Figure 2. Excitation spectrum of DTB vapor in a jet in the $1^1A_g \rightarrow 2^1A_g$ and $1^1A_g \rightarrow 1^1B_u$ regions. Emission was monitored from 400 to 800 nm using a glass filter (Toshiba L-42).

3. Results and Discussion

3.1. Excitation and Emission Spectra in a Jet. *α,ω-Dithienylbutadiene (DTB).* There are three possible conformations (rotational isomers or rotamers) for DTB, as illustrated in Figure 1. These are tentatively named anti−anti (C_{2h}), anti−syn, and syn−syn (C_{2h}) conformers, depending on the C=C double bond orientation in the two thienyl rings. The results of the DFT calculation at the B3LYP/6-311++G** level for DTB in the ground state show that the anti−anti is the most stable conformer and is lower in energy by 704 and 352 cm^{-1} than the syn−syn and anti−syn conformers, respectively. Similar results were obtained for the stability of the three conformers with the semiempirical calculations such as AM1, PM3, and INDO/3, although the energy differences among the conformers are slightly different from the DFT outputs. In the case of AM1 calculation, for example, the energy difference between the anti−anti and anti−syn and that between the anti−anti and syn−syn conformers of DTB are 585 and 626 cm^{-1}, respectively. In any case, the order of the stability of the three conformers of DTB is considered to be syn−syn > anti−syn > anti−anti in the ground state. It should be noted here that the singlet electronic states of the anti−anti and syn−syn comfomers can be expressed by the symmetry notations such as ^{1}Ag and ^{1}Bu, although this does not apply to the anti−syn conformer.

Excitation and fluorescence spectra of DTB vapor in a jet are shown in Figures 2 and 3, respectively. The excitation spectrum consists of sharp bands starting from 25470.5 cm^{-1} and comparatively broad and intense bands starting from about

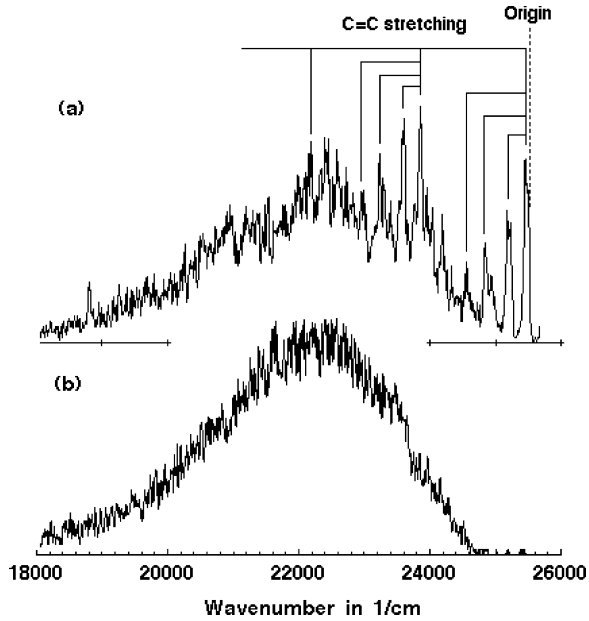

Figure 3. Dispersed fluorescence spectra of DTB vapor in a jet following the excitation into the false 2^1A_g origin (25471 cm^{-1}) (a) and a band in the 1^1B_u region (28310 cm^{-1}) (b).

28300 cm^{-1}. In light of the absorption spectrum of DTB in the static vapor phase shown later (see Figure 8), the latter intense bands are assigned as those originating from the transition to the S_2 state. The first band observed at 25470.5 cm^{-1} in the excitation spectrum in Figure 2 is assigned to the false origin of the forbidden $S_0(1^1A_g) \rightarrow S_1(2^1A_g)$ transition of the anti−anti conformer on the basis of the following reasons:

(1) The fluorescence lifetime obtained by the excitation at the false origin of the $S_1(2^1A_g)$ state (25471 cm^{-1}) is obtained to be 12 ns. The molar extinction coefficient of DTB at the S_2 absorption maximum is 19570 $M^{-1}cm^{-1}l$ in hexane at room temperature, which leads to the intrinsic radiative lifetime of 2 ns ($k_{F2} = 5 \times 10^8$ s^{-1}) based on the Strickler−Berg equation.[25] Obviously, the measured fluorescence lifetime is longer than that estimated from the oscillator strength of the S_2 state, despite the fact that the fluorescence quantum yield is less than unity.

(2) The location of the false origin of the S_1 (2^1A_g) state (25471 cm^{-1}) agrees almost exactly with that determined in a low temperature matrix (25500 cm^{-1}),[16] and there are no bands observed at energies below the false origin in the excitation spectrum (Figure 2).

(3) The vibrational frequencies observed in the dispersed fluorescence spectrum in Figure 3 following the excitation into the false 2^1A_g origin (25470.5 cm^{-1}) agree well with those obtained by the DFT calculations at the B3LYP/6-311++G** level for the anti−anti conformer but do not agree as a whole with those obtained for the syn−syn or anti−syn conformer (see Table 1).

The intensity of the false 2^1A_g origin in the excitation spectrum is comparatively high as compared with that of diphenylbutadiene (see Figure 2).[15] The appearance of the strong peak of the false 2^1A_g origin is considered to be mainly due to the presence of the fast nonradiative transition from the $S_1(2^1A_g)$ state at higher excitation energies (the peak intensity of the excitation spectrum in the $S_1(2^1A_g)$ region tends to decrease with increasing excitation energy). As will be shown later in detail, the fluorescence yield of DTB decreases significantly with increasing excitation energy (see Figure 9). The false $S_1(2^1A_g)$ origin is located approximately 2800 cm^{-1} below the $S_2(1^1Bu)$ origin (Figure 2). The theoretical values for the $2^1A_g-1^1B_u$ energy separation reported by Negri and Zgierski for the anti−anti conformer of DTB are 1371 cm^{-1} (S_0 geometry, vertical), 2500 cm^{-1} (S_1 geometry, vertical), 3952 cm^{-1} (S_2 geometry, vertical), and 5485 cm^{-1} (adiabatic),[26] which seem to be in reasonable agreement with the observed value of about 2800 cm^{-1} in a jet.

TABLE 1: Shifts $\Delta\nu$ (cm^{-1}) from the False 2^1A_g Origin (25470.5 cm^{-1}) for the Observed Fluorescence Excitation Bands of DTB Vapor in a Jet

$\Delta\nu^a$	assignment	$\Delta\nu$ in matrix at 4.2 K[b]	calculated $\Delta\nu^c$
0	false 2^1Ag origin	0	
115.1		108	106, 106, 123
230.1			231, 231, 245
233.2			231, 231, 245
254.0			
492.2			443, 451, 488
498.9			
561.0	ring		559, 585, 575
590.2			
665.0	ring	679	660, 693, 745
760.7			
1149.8	C−C str.		1159, 1164, 1231
1319.2	C−C str.		1313, 1320, 1359
1653.2	C=C str.		1838, 1815, 1674
1674.8			
1710.6	1149.8 + 561.0		
1730.0			
1735.8	1149.8 + 590.2		
1746.0			
1773.4			
1825.0			
1847.8			
1879.5	1319.2 + 561.0		
1907.5	1653.1 + 254.0		
1928.6	1319.2 + 665.0		

[a] Accuracy of ±0.2 cm^{-1}. [b] Taken from ref 16. [c] Taken from ref 26. Tentative correspondences. The three values correspond to the ones obtained by different calculation methods.

The weak features seen between 25471 and 27500 cm^{-1} in the excitation spectrum may involve the vibronic bands inherent to the thienyl rings but may involve also the bands of the conformers other than the anti−anti form. The comparatively strong band at 27123.2 (1652.7) cm^{-1} can be assigned to the C=C stretching mode of the anti−anti conformer that dominates the vibronic development of linear polyene absorption spectra, while the bands at 26619.9 (1149.4) or 26789.3 (1318.8) cm^{-1} can be assigned to the C−C stretching modes, with the wavenumber shift from the false 2^1A_g origin being shown in parentheses. The 2^1A_g origin is estimated to be located slightly below the false origin in the excitation spectrum, and the vibrational mode responsible for promoting the $1^1A_g-2^1A_g$ transition must be the one with the b_u symmetry and with the DFT calculated frequency of 48.8 cm^{-1} in the ground state. The bands observed in the excitation spectrum are summarized in Table 1 along with the calculated frequencies reported by Negri and Zgierski.[26] Although there is general agreement between the calculated and observed frequencies, some of the observed bands do not agree in position with the calculated ones. This may be due to the involvement of the peaks of the conformers other than the anti−anti, since we have monitored the emission through a glass filter.

The fluorescence spectrum following the excitation into the false 2^1A_g origin shows band structures, while that following the excitation of the 1^1B_u state is significantly broad. This observation demonstrates that the $S_1(2^1A_g)$ fluorescence origi-

TABLE 2: Frequencies (cm^{-1}) and Assignments of the Observed Fluorescence Bands of DTB Vapor in a Jet Following Excitation into the False 2^1A_g Origin at 25471 cm^{-1}

frequency[a]	ΔE	intensity	assignment	ν_{calc}[b]	in solid matrix[c]
25471	0	0.78	false origin		0
25361	110	0.07	a_g ring, bend.	106.9	111
25201	270	0.56	b_u ring, bend.	265.0	
24981	490	0.18	a_u ring, deform.	494.2	
24941	530	0.29	b_g ring, deform.	516.7	
24841	630	0.42	a_g ring, deform.	625.3	621
24561	910	0.33	b_g ring, C−H bend.	907.6	
24326	1145	0.33	a_g C−C str.	1153.5	1140
24256	1215	0.31	b_u C−C str.	1216.0	
24186	1285	0.56	a_g C−C str.	1298.8	1289
24031	1440	0.58	b_u ring, deform.	1440.9	1437
23926	1545	0.64	110 + 1440		1547
23851	1620	1.00	a_g C=C str.	1621.8	1615
23746	1725	0.56	1620 + 110		1727
23586	1885	0.93	1620 + 270		
23391	2080	0.60	1620 + 490		2056
23311	2160	0.71	1620 + 530		
23221	2250	0.80	1620 + 630		2334
22941	2530	0.64	1620 + 910		
22566	2905	0.80	1620 + 1285		
22411	3060	0.87	1620 + 1440		
22201	3270	0.84	1620 × 2		
21527	3944	0.62			
21187	4284	0.58			

[a] Accuracy of ±4 cm^{-1}. [b] Obtained by DFT calculation at the B3LPY/6-311++G** level. Calculated DFT frequencies are modulated using the relation $\nu_{calc} = 1.0087 \times \nu_{DFT} - 0.0000163 \times \nu_{DFT}^2$, in order to include the anharmonicity factor. [c] Data from ref 16.

nates from the higher vibronic levels of the S_1 state in the case of the excitation into S_2. The vibrational frequencies of the fluorescence bands following the excitation of the false S_1 (2^1A_g) origin are summarized in Table 2 along with the assignments. The vibronic bands in the fluorescence spectrum involve both the polyene and thienyl-ring vibrations.

α,ω-Dithienylethylene (DTE). There are three possible conformers also for DTE, as illustrated in Figure 1 for DTB. The results of the DFT calculation at the B3LYP/6-311++G** level show that the anti−anti conformer is lower in energy by 720 and 384 cm^{-1} than the syn−syn and anti−syn conformers, respectively. Similar results were obtained concerning the stability of the conformers with the semiempirical calculations such as AM1, PM3, and INDO/3, although the energy differences among the conformers are slightly different from the DFT outputs. Therefore, the main conformer in the ground state is considered to be the anti−anti conformer also for DTE. Excitation and fluorescence spectra of DTE vapor in a jet are shown in Figures 4 and 5, respectively. Two progressions with different intervals are observed in the excitation spectrum. On the basis of the vibronic structure in the excitation spectrum, both of the two progressions are assigned to the $S_0 \rightarrow S_1$ transition ($1^1A_g \rightarrow 1^1B_u$ transition for the anti−anti conformer) corresponding to the two different conformers. In order to assign these excitation bands, the dispersed fluorescence spectra were measured following the excitation of the different vibronic bands (Figure 5). All of the fluorescence spectra following the excitation of the bands in the progression starting from 28648 cm^{-1} showed a frequency of 183 (182.8) cm^{-1} which is characteristic of the anti−syn conformer. On the other hand, the fluorescence following the excitation of the bands in the progression starting from 28966 cm^{-1} showed a frequency of 158 (158.3) cm^{-1} characteristic of the anti−anti conformer, with the DFT calculated frequencies shown in parentheses. Thus, the

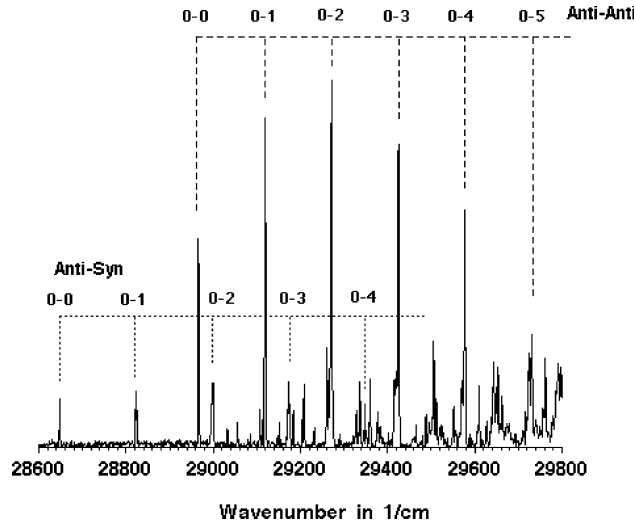

Figure 4. Excitation spectrum of DTE vapor in a jet. Emission was monitored from 400 to 800 nm using a glass filter (Toshiba L-42).

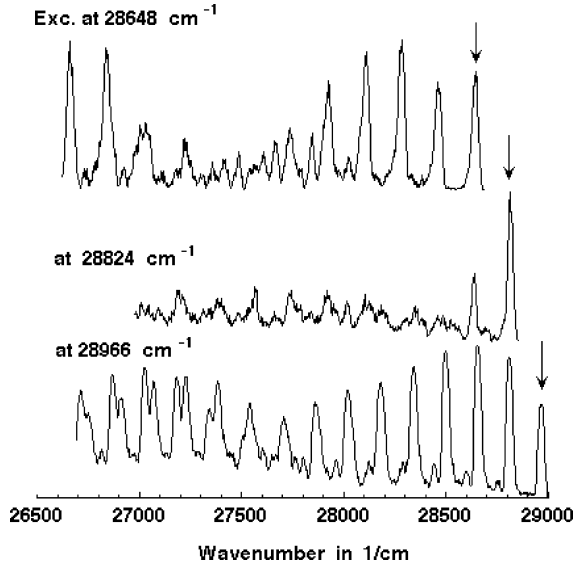

Figure 5. Dispersed fluorescence spectra of DTE vapor in a jet obtained by the excitation into the different vibronic levels. The locations of the excitation are indicated by arrows.

former bands are assigned to those of the anti−syn conformer and the latter to the anti−anti conformer. The vibrational frequencies of the bands observed in the excitation spectrum of DTE are summarized in Table 3, and those observed in the fluorescence spectra following the excitation into the 1^1Bu origins of the two different conformers are shown in Tables 4 and 5 along with the assignments. As for the syn−syn conformer of DTE, the contribution to the observed spectra is considered to be small due to the higher energy in the ground state (720 cm^{-1} higher in energy than the anti−anti conformer based on the DFT calculation).

3.2. Photophysics and Spectroscopy of DTB and DTE Vapors in the Static Vapor Phase. Figure 6 shows the absorption, excitation, and emission spectra of DTB vapor at different temperatures, where the spectra were obtained in the presence of an added foreign gas. There is a large Stokes shift near 7000 cm^{-1} between the measured absorption and emission spectra. In light of the emission spectra in a jet, most of the intensity in the emission spectra is considered to be originating from the $S_1 \rightarrow S_0$ transition. Closer inspection of the emission spectra reveals a weak shoulder emission band near 26000 cm^{-1}

TABLE 3: Frequencies (cm^{-1}) and Assignments of the Observed Fluorescence Excitation Bands of DTE Vapor in a Jet

	assignment	
frequency[a]	anti−syn	anti−anti
28648	S_1 origin (anti−syn)	
28824	176 (ring, bend.)	
28966		$S_1(1^1Bu)$ origin (anti−anti)
28999	176 × 2	34 (ring, tor.)
29032		66 (ring, bend.)
29055		89 (ring, bend.)
29080		114
29106		141
29112		146
29118		152 (ring, bend.)
29152		152 + 34
29175	176 × 3	
29184		152 + 66
29207		152 + 89
29232		152 + 114
29261		152 + 141
29265		152 + 146
29271		152 × 2
29336		152 × 2 + 66
29350	176 × 4	
29362		152 × 2 + 89
29384		152 × 2 + 114
29415		152 × 2 + 141
29421		152 × 2 + 146
29424		152 × 3
29460		152 × 3 + 34
29489		152 × 3 + 66
29512		152 × 3 + 89
29522	176 × 5	
29569		152 × 3 + 141
29572		152 × 3 + 146
29577		152 × 4
29610		152 × 4 + 34
29643		152 × 4 + 66
29663		152 × 4 + 89
29717		152 × 4 + 141
29725		152 × 4 + 146
29730		152 × 5
29762		152 × 5 + 34
29797		152 × 5 + 66
29820		152 × 5 + 89
29873		152 × 5 + 141
29884		152 × 6

[a] Accuracy of ±2 cm^{-1}.

on the high-energy side of the S_1 fluorescence. This weak shoulder band is assigned to the fluorescence from the S_2 state (the 1^1Bu state for the anti−anti conformer) on the basis of the following observations:

(1) The weak shoulder band appears to be the mirror image of the origin of the $S_0 \rightarrow S_2$ absorption.

(2) The excitation spectra at high total pressure obtained by monitoring the weak shoulder emission and the main emission are almost identical, and these excitation spectra correspond nearly to the absorption spectrum. As will be mentioned later in detail, the excitation spectrum at low pressure does not agree with the absorption spectrum due to the presence of the fast internal conversion to the ground state, although the excitation spectrum tends to resemble the absorption spectrum with increasing pressure.

(3) The relative intensity of the weak shoulder emission increases with increasing temperature.

In order to confirm the present assignment, the relative emission intensities measured as a function of temperature have been analyzed quantitatively. That is, the S_1 and S_2 fluorescence spectra have been fitted by sums of Gaussians. The intensity $I(\nu)$ of the spectrum at wavenumber ν was assumed to have the form $I(\nu) = \sum_i I_i(\nu_i) \exp[-(\nu - \nu_i)^2/\sigma^2]$. In the case of fluorescence spectra of DTB, when six Gaussians, i.e., the origin, one and two quanta of the symmetric C—C (1153 cm^{-1}) and C═C (1622 cm^{-1}) stretching modes, and the combination of the stretching modes, were fit to the first 6000 cm^{-1} of the

TABLE 4: Frequencies (cm^{-1}) and Assignments of the Observed Fluorescence Bands of DTE Vapor in a Jet Obtained by the Excitation at the 1^1B_u Origin of the Anti−Anti Conformer

frequency[a]	ΔE (cm^{-1})	assignment	calculated frequency[b]	Raman[c]
28966	0	1^1Bu origin (anti−anti)		
28808	158	158 (a_g ring, bend.)	158.3	
28652	314	158 × 2		
28495	471	158 × 4		
28181	785	158 × 5		
28019	947	158 × 6		
27861	1105	158 × 7		
27705	1261	158 × 8		
27537	1429	1429 (a_g), 158 × 9	1432.9	1420
27383	1583	1429 + 158, 158 × 10		
27336	1630	1630 (a_g C═C str.)	1634.5	1618
27226	1738	1429 + 158 × 2		
27179	1783	1630 + 158		
27069	1897	1429 + 158 × 3		
27028	1938	1630 + 158 × 2		
26913	2053	1429 + 158 × 4		
26867	2099	1630 + 158 × 3		
26748	2218	1429 + 158 × 5		
26713	2253	1630 + 158 × 4		

[a] Accuracy of ±2 cm^{-1}. [b] Obtained by DFT calculation at the B3LPY/6-311++G** level. Calculated DFT frequencies are modulated using the relation $\nu_{calc} = 1.0087 \times \nu_{DFT} - 0.0000163 \times \nu_{DFT}^2$, in order to include the anharmonicity factor. [c] Taken from ref 27. In the Raman spectrum, both of the anti−anti and anti−syn conformers are considered to coexist.

TABLE 5: Frequencies (cm^{-1}) and Assignments of the Observed Fluorescence Bands of DTE Vapor in a Jet Obtained by the Excitation at the S_1 Origin (28648 cm^{-1}) of the Anti−Syn Conformer

frequency[a]	ΔE (cm^{-1})	assignment	calculated frequency[b]	Raman[c]
28648	0	1^1Bu origin (anti−syn)		
28465	183	183 (ring)	182.8	
28283	365	183 × 2		
28103	545	183 × 3		
28023	625	625 (ring, deform.)	625.5	635
27922	726	183 × 4		
27843	805	625 + 183		
27734	914	183 × 5		
27663	985	625 + 183 × 2		
27560	1088	183 × 6		
27485	1163	625 + 183 × 3		
27420	1228	1228 (ring, C—H bend.)	1226.3	1244
27358	1290	183 × 7		
27218	1430	1430 (ring, C═C str.)	1430.0	1420
27110	1538	1538 (ring, C═C str.)	1538.9	
27035	1613	1430 + 183		
27020	1628	1628 (polyene, C═C str.)	1628.5	1618
26840	1808	1628 + 183		
26660	1988	1628 + 183 × 2		

[a] Accuracy of ±2 cm^{-1}. [b] Obtained by DFT calculation at the B3LPY/6-311++G** level. Calculated DFT frequencies are modulated using the relation $\nu_{calc} = 1.0087 \times \nu_{DFT} - 0.0000163 \times \nu_{DFT}^2$, in order to include the anharmonicity factor. [c] Taken from ref 27. In the Raman spectrum, both of the anti−anti and anti−syn conformers are considered to coexist.

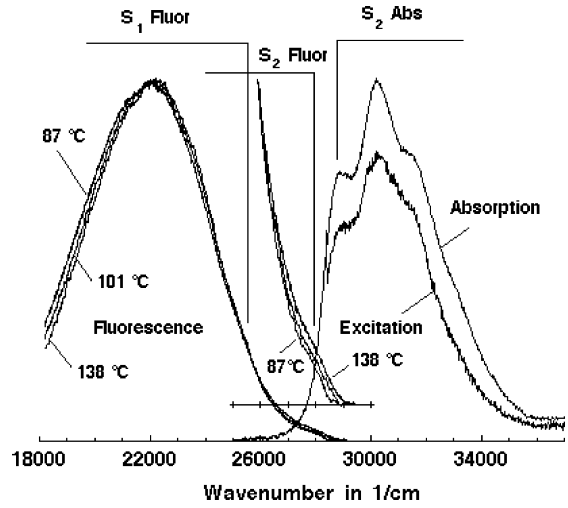

Figure 6. Absorption, excitation, and fluorescence spectra of DTB in the static vapor phase in the presence of 380 Torr perfluorohexane as a buffer gas at different temperatures (87, 101, and 138 °C). Fluorescence spectra were obtained by excitation at 320 nm, and excitation spectra were obtained by monitoring the S_2 fluorescence at 357 nm. All of the spectra are normalized to a common magnitude, except for the excitation spectra which are multiplied by 0.8.

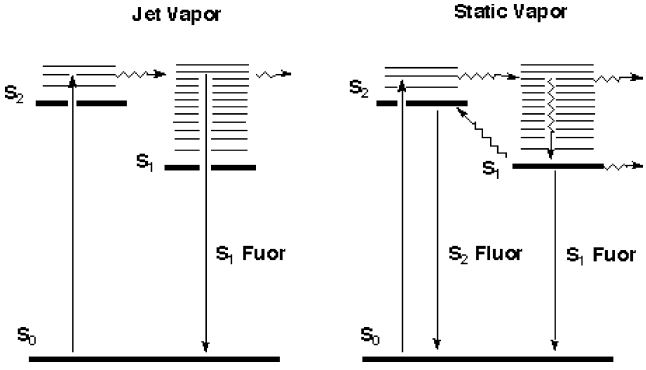

Figure 7. Schema showing relaxation processes of DTB in a jet (left) and in the static vapor phase (right).

corrected fluorescence spectra, the measured and calculated spectra were almost indistinguishable from each other. In order to derive more accurate intensity estimates for the S_1 fluorescence, the $S_0 \rightarrow S_2$ absorption spectrum reflected so as to match the reflected origin to the origin of S_2 fluorescence was subtracted from the measured fluorescence, and the resulting difference spectrum was refit by Gaussians to obtain the intensity of the Gaussian corresponding to the $S_1(2^1A_g)$ fluorescence alone.

Schema showing the relaxation processes of DTB both in a jet and in the static vapor phase are presented in Figure 7. In the case of the jet-cooled environment, the emission originates only from the S_1 state, but in the static vapor phase at ambient temperatures, the emission originates from S_1 accompanied by the weak S_2 fluorescence which occurs as the result of the thermal activation of S_1. When two closely located electronic states (in the present case, S_1 and S_2) are in thermodynamic equilibrium, the quantum yield ratio of the emission from the lower state (S_1) to that from the upper state (S_2), Φ_{F2}/Φ_{F1}, is given approximately by $\Phi_{F2}/\Phi_{F1} = (k_{F2}/k_{F1}) \times \exp[\Delta E/kT]$, where ΔE is the S_1-S_2 energy separation, k_{F1} and k_{F2} are, respectively, the radiative rate constants of the S_1 and S_2 states, and T is the absolute temperature. We have used the fitted band intensities of the S_1 and S_2 fluorescence origin bands (I_{F1} and I_{F2}), instead of Φ_{F1} and Φ_{F2}. The ΔE value obtained from the

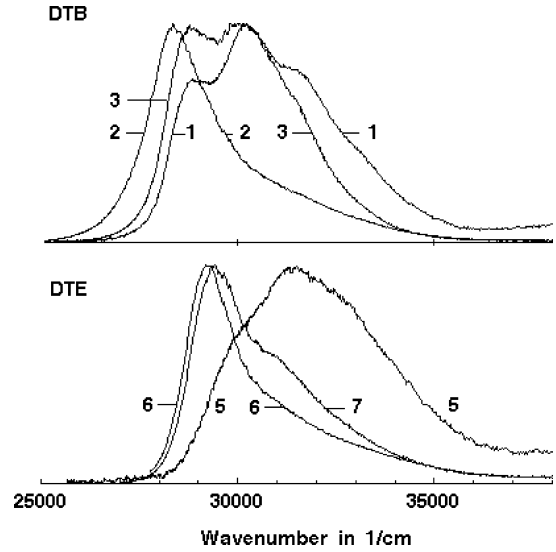

Figure 8. Corrected excitation spectra of DTB (upper panel) and DTE (lower panel) vapors at different pressures (2, 3, 6, and 7) along with the absorption spectra (1 and 5): 2 and 6, pure samples without buffer gas; 3 and 7, with 400 Torr perfluorohexane as a buffer gas. The excitation spectra were measured at 138 °C, and the absorption spectra were measured at 90 °C. All of the spectra are normalized to a common magnitude.

logarithmic values of I_{F2}/I_{F1} plotted against $1/T$ are 2100 ± 400 cm^{-1}, which is in reasonable agreement with that estimated from the data in a jet ($\sim$2800 cm^{-1}).

As shown in a previous paper, in the case of DTE vapor, such a weak band is not observed and the emission appears to be the mirror image of the strong $S_0 \rightarrow S_1$ absorption with a sufficient overlapping between the emission and absorption spectra.[19] Therefore, the emission of DTE vapor can be regarded as the fluorescence from the optically allowed S_1 (1^1Bu for the anti−anti and syn−syn conformers) state.

We have investigated the excitation energy dependence of the fluorescence quantum yields of DTB and DTE in the static vapor phase at low pressure, since it is normally difficult to investigate this property quantitatively in a jet. Figure 8 shows corrected excitation spectra of DTB and DTE vapors at different pressures along with the absorption spectra. The pressures of pure DTB and DTE vapors at the temperatures employed in the measurements are on the order of 10^{-2} Torr. In the case of DTB vapor, the relative intensity of the excitation spectrum at higher excitation energies at low pressure is markedly low as compared with that of the absorption spectrum, but the excitation spectrum tends to resemble the absorption spectrum with increasing pressure. A similar future is observed also for DTE vapor in the excitation spectrum. It may be noted that the excitation envelope of pure DTE in the static vapor phase is nearly the same as that in a jet. Further, at low pressure without the buffer gas, the fluorescence maxima of DTB and DTE vapors tend to shift to the red with increasing excitation energy, suggesting the occurrence of the fluorescence from the unrelaxed vibronic levels in S_1.

In Figure 9, the relative fluorescence quantum yields are shown as a function of the excitation energy for DTB and DTE vapors at different pressures. These yields were obtained by dividing the corrected excitation spectrum by the absorption spectrum. It is seen in Figure 9 that the fluorescence yield decreases almost monotonously with increasing excitation energy and that the decrease is more pronounced as the pressure is lowered. These observations indicate that the fast internal

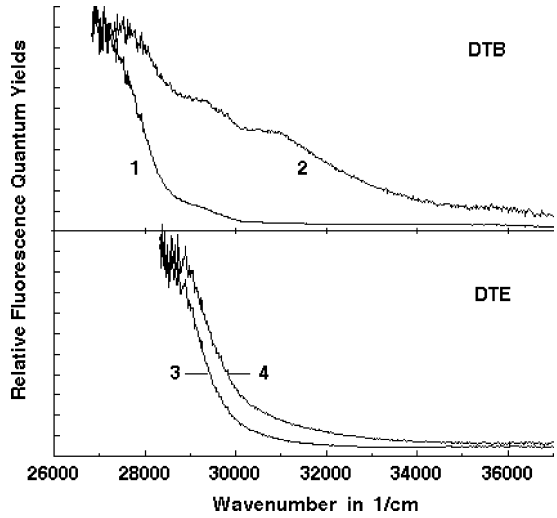

Figure 9. Relative fluorescence quantum yields shown as a function of the excitation energy for DTB (upper panel) and DTE (lower panel) vapors at different pressures: 1 and 3, pure samples without buffer gas; 2 and 4, with 280 Torr perfluorohexane as a buffer gas.

conversion to the ground state is taking place from the fluorescent state, which may possibly include the photoisomerization, and that the internal conversion is competing with the collisional deactivation to the lower vibronic levels of the fluorescent S_1 state.

In the case of static vapor, the coexistence of the two or three conformers might be considered. The Boltzmann distribution indicates that the anti−anti:anti−syn:syn−syn ratio in the ground state of DTB at 120 °C is 1.0:0.27:0.08, assuming an energy difference between the anti−anti and anti−syn conformers and between the anti−anti and syn−syn conformers of 352 and 704 cm^{-1}, respectively. Thus, in the static vapor phase, the observed emission presumably consists of the mixture of the fluorescence from two or three conformers, although the main conformer in the ground state is considered to be the anti−anti conformer.

4. Conclusions

Fluorescence and fluorescence excitation spectra have been measured for *trans*-1,4-di(2-thienyl)-1,3-butadiene (DTB) and *trans*-1,2-di(2-thienyl)ethylene (DTE) in a jet cooled He expansion as well as in the static vapor phase. The emission of DTB consists of the S_2 and S_1 fluorescence in the static vapor phase, while it consists of solely the S_1 fluorescence in a jet, where the S_1 and S_2 states correspond, respectively, to the 2^1A_g and 1^1B_u states for the anti−anti conformer. The emission of DTE consists of solely the S_1 fluorescence in the static vapor phase as well as in a jet, where the S_1 state corresponds to the 1^1Bu state for the anti−anti conformer in a jet. The fluorescence quantum yields of DTB and DTE vapors are found to decrease significantly with increasing excitation energy. In a jet, the conformer-specific fluorescence was observed for DTB and DTE vapors. The false $S_1(2^1A_g)$ origin of the most stable anti−anti conformer of DTB vapor was observed at 25470.5 cm^{-1} in a jet, which is located approximately 2800 cm^{-1} below the $S_2(1^1B_u)$ origin. The emission of DTE is assigned as the S_1 fluorescence both in the static vapor phase and in a jet. The S_1 origins of the anti−syn and anti−anti conformers of DTE vapor were observed at 28648 and 28966 cm^{-1}, respectively, in a jet. It is inferred from the excitation measurements that the 2^1A_g state of the anti−anti conformer of DTE vapor is located at energies above the $S_1(1^1B_u)$ state. The prominent features of the photophysics and spectroscopy of dithienylpolyenes, as compared with those of diphenylpolyenes and unsubstituted polyenes, are that there are more than two rotational isomers and that both of the polyene and thienyl-ring vibrations are involved in the spectra.[15,28,29]

Acknowledgment. We are indebted to Professor Isamu Suzuka of Nihon University for encouragement.

References and Notes

(1) Hudson, B. S.; Kohler, B. E. *Chem. Phys. Lett.* **1972**, *14*, 299.
(2) Hudson, B. S.; Kohler, B. E. *J. Chem. Phys.* **1973**, *59*, 4984.
(3) Hudson, B. S.; Kohler, B. E.; Shulten, K. *Excited States* **1983**, *6*, 1.
(4) Kohler, B. E. *Chem. Rev.* **1993**, *93*, 41, and references cited therein.
(5) Horwitz, J. S.; Itoh, T.; Kohler, B. E.; Spangler, C. W. *J. Chem. Phys.* **1987**, *87*, 2433.
(6) Kohler, B. E.; Spanglar, C. W.; Westerfield, C. *J. Chem. Phys.* **1988**, *89*, 3506.
(7) Itoh, T.; Kohler, B. E. *J. Phys. Chem.* **1987**, *91*, 1760.
(8) Itoh, T. *J. Chem. Phys.* **2003**, *119*, 4516.
(9) Itoh, T. *Chem. Phys. Lett.* **2003**, *377*, 577.
(10) Itoh, T. *J. Chem. Phys.* **2004**, *121*, 6956.
(11) Itoh, T. *J. Chem. Phys.* **2005**, *123*, 64302–1.
(12) Snyder, R.; Arvidson, E.; Foote, C.; Harrigan, L.; Christensen, R. L. *J. Am. Chem. Soc.* **1985**, *107*, 4117.
(13) Bachilo, S. M.; Spangler, C. W.; Gillbro, T. *Chem. Phys. Lett.* **1998**, *283*, 235.
(14) Shepanski, J. F.; Keelan, B. W.; Zewail, A. H. *Chem. Phys, Lett.* **1983**, *103*, 9.
(15) Heimbrook, L. A.; Kohler, B. E.; Spiglamin, T. A. *Proc. Natl. Acad. Sci. U.S.A.* **1983**, *80*, 4580.
(16) Birnbaum, D.; Kohler, B. E.; Spangler, C. W. *J. Chem. Phys.* **1991**, *94*, 1684.
(17) Cooper, T. M.; Natarajan, L. V.; Sowards, L. A.; Spangler, C. W. *Chem. Phys. Lett.* **1999**, *310*, 508.
(18) Bartocci, G.; Spalletti, A.; Becker, R. S.; Elisei, F.; Floridi, S.; Mazzucato, U. *J. Am. Chem. Soc.* **1999**, *121*, 1065.
(19) Itoh, T.; Yamaji, M. *J. Phys. Chem. A* **2008**, *112*, 13413.
(20) Okuyama, K.; Numata, Y.; Odawara, S.; Suzuka, I. *J. Chem. Phys.* **1998**, *109*, 7185.
(21) Itoh, T. *J. Fluoresc.* **2006**, *16*, 739.
(22) Lippert, E.; Nagele, W.; Seibold-Blankenstein, I.; Staiger, U.; Voss, F. *Z. Anal. Chem.* **1959**, *170*, 1.
(23) Frisch, M. J.; Trucks, G. W.; Schlegel, H. B.; Scuseria, G. E.; Robb, M. A.; Cheeseman, J. R.; Montgomery, J. A.; Vreven, T., Jr.; Kudin, K. N.; Burant, J. C.; Millam, J. M.; Iyengar, S. S.; Tomasi, J.; Barone, V.; Mennucci, B.; Cossi, M.; Scalmani, G.; Rega, N.; Petersson, G. A.; Nakatsuji, H.; Hada, M.; Ehara, M.; Toyota, K.; Fukuda, R.; Hasegawa, J.; Ishida, M.; Nakajima, T.; Honda, Y.; Kitao, O.; Nakai, H.; Klene, M.; Li, X.; Knox, J. E.; Hratchian, H. P.; Cross, J. B.; Adamo, C.; Jaramillo, J.; Gomperts, R.; Stratmann, R. E.; Yazyev, O.; Austin, A. J.; Cammi, R.; Pomelli, C.; Ochterski, J. W.; Ayala, P. Y.; Morokuma, K.; Voth, G. A.; Salvador, P.; Dannenberg, J. J.; Zakrzewski, V. G.; Dapprich, S.; Daniels, A. D.; Strain, M. C.; Farkas, O.; Malick, D. K.; Rabuck, A. D.; Raghavachari, K.; Foresman, J. B.; Ortiz, J. V.; Cui, Q.; Baboul, A. G.; Clifford, S.; Cioslowski, J.; Stefanov B. B.; Liu, G.; Liashenko, A.; Piskorz, P.; Komaromi, I.; Martin, R. L.; Fox, D. J.; Keith, T.; Al-Laham, M. A.; Peng, C. Y.; Nanayakkara, A.; Challacombe, M.; Gill, P. M. W.; Johnson, B.; Chen, W.; Wong, M. W.; Gonzalez, C.; Pople, J. A. *Gaussian 03*, revision B.05; Gaussian, Inc.: Pittsburgh, PA, 2003.
(24) Yoshida, H.; Takeda, K.; Okamura, J.; Ehara, A.; Matsuura, H. *J. Phys. Chem. A* **2002**, *106*, 3580.
(25) Strickler, S. J.; Berg, R. A. *J. Chem. Phys.* **1962**, *37*, 814.
(26) Negri, F.; Zgierski, M. Z. *J. Chem. Phys.* **2001**, *115*, 1298.
(27) Mevellec, J. Y.; Buisson, J. P.; Lefrant, S. *Syn. Met.* **1991**, *41*, 283.
(28) Kohler, B. E.; Spiglamin, T. A. *J. Chem. Phys.* **1984**, *80*, 5465.
(29) Heimbrock, L. A.; Kenny, J. E.; Kohler, B. E.; Scott, G. W. *J. Chem. Phys.* **1981**, *75*, 4338.

JP901180A